

Ultrasensitive multi-mode ESR probed ferromagnetic two-level system of Mn^{4+} impurity ion in the insulated MnO_6 complex of $SrLaAlO_4$ at 20 mK

M. A. Hosain^{1, a)}

ARC Centre of Excellence for Engineered Quantum Systems, School of Physics, University of Western Australia, 35 Stirling Highway, Crawley WA 6009, Australia.

Ultrasensitive multi-mode electron spin resonance spectroscopy in the $SrLaAlO_4$ dielectric resonator at 20 mK reveals ferromagnetic states of Mn^{4+} impurity ion. The formation of ferromagnetic states in the MnO_6 complex implies to oxygen deficiency of this multi-valence Mn^{4+} ion. Experiment results supports that an intricate electronic hybridization in MnO_6 structural instability is related to Pseudo Jahn-Teller effect. Measured dipolar hyperfine structure parameter of nucleus is $P_{||} = -3.7 \times 10^{-4} \text{ cm}^{-1}$. Mean inverse third power of the electron distance is $\langle r_q^{-3} \rangle = 3.325 \text{ a.u.}$ assuming nuclear electric quadrupole moment $Q = +0.33(1) \text{ barn}$. In such a state, giant g-factor is observed due to magneto (ferromagnetic) impedance taking in to account a two-level system on the adiabatic-potential-energy-surface. The spins exhibited parity is opposite in the interaction of highest-occupied-molecular-orbital and lowest-unoccupied-molecular-orbital coupling.

A. Introduction:

Ultrasensitive electron spin resonance (ESR) with high precision in dielectric crystal multi-mode resonators assimilating as hybrid-quantum system is a road-map for the development of quantum technologies¹⁻⁴. This experimental study is on impurity paramagnetic ion's unpaired electron spin states using electron spin resonance (ESR) spectroscopy in a suitable dielectric crystal resonator exciting microwave whispering gallery (WG) modes⁵⁻⁷. WG multi-mode ESR spectrum works as a direct probe providing information of electronic and magnetic states of paramagnetic impurity ions⁸. In this process, Mn^{4+} ion has been detected in the dielectric single crystal $SrLaAlO_4$ (SLA), and analysed taking into account an intricate electronic hybridization due to its extra charge in MnO_6 complex at 20 millikelvin (mK). This $d-p$ metal-ligand orbital hybridization is mediated in MnO_6 structural instability, and plays a vital role in the mechanism of spontaneous polarization and/or magnetization forming two-level system on the adiabatic potential energy surface (APES)⁹. Naturally, paramagnetic ion's three phenomena ferro-electricity, magnetization, and spin-crossover are observed as coexisted¹⁰. Ohkoshi et al.¹¹ demonstrated unpaired electrons as a spin-crossover magnet in the mechanism of light induced phase transition. Such a transition process can be used to monitor magnetization saturation (M_s), Curie temperature (T_c), coercive (magnetic) field (H_c) and/or the magnetic pole¹¹. Optical spectroscopy and X-ray diffraction (XRD) results are available providing localization information of Mn^{4+} ion in this type of crystal^{12,13}.

Many studies have been devoted towards better understanding of the main mechanisms governing electron delocalization and electron intervalence absorptions of transition metals in metal-ligand complexes^{14,15}. These transition metal based crystals like $LaMnO_3$ exhibits interesting magnetic behaviours, such as, mono-metallic

complexes in the crystal exhibiting single ion magnetic (SIM) behaviour^{14,16}, and two or more metal sites of varying oxidation numbers (known as mixed valence (MV) sites^{16,17}) exhibits single molecular magnet (SMM) behaviour^{14,17}. This is essentially important due to the fact that these metal-ligand complex structures possess several potential applications in quantum technology^{14,15}. However these characteristics due to their intrinsic magnetic properties, SMMs are distinctly detected only at liquid helium temperatures^{14,18}. Among the MV metal complexes, dual-exchange (DE)^{14,16} is generated due to the presence of an itinerant electron in two different valence sites in the crystal. As instance, electron exchanges between two neighbouring sites Mn^{3+} and Mn^{4+} in the $Mn-O-Mn$ chain of $LaMnO_3$ crystal¹⁹. The MV metal ion complexes exhibit coupling of electron movement with the structural distortion, and subsequently affects the degree of localization of the extra electron^{14,20,21}. The oxidation variation of MV sites of the metal-ligand complex produces distortions as Jahn-Teller effect (JTE) within trigonal plane of lower symmetry, and can be confirmed from ESR spectrum^{15,19,20}.

Intriguingly, we examine an insulated octahedral mono-metallic complex MnO_6 in $SrLaAlO_4$ where Al^{3+} ion is substituted by Mn^{4+} ion^{12,17}. In this case the manganese ion shows multi-valence behaviour instead of MV behaviour. Interesting magnetic behaviours of this type of transition metal complex are observed in a linear combination of atomic orbitals. Neither the DE mechanism which is a type of magnetic exchange (whether materials are ferromagnetic or antiferromagnetic) that may arise between MV ions in the $Mn-O-Mn$ link, nor the super-exchange (SE) (or Kramers-Anderson super-exchange) which is a strong (usually) antiferromagnetic coupling between two next-to-nearest neighbour cations, is possible for an insulated MnO_6 individual unit in $SrLaAlO_4$. We will justify this multi-valence manganese ion in a metal-ligand charge transfer (oxidation variation) produced spontaneous magnetization with the measured spin-Hamiltonian parameters along with site symmetry²²⁻²⁵.

^{a)} Electronic mail: akhter361@yahoo.co.uk

The magnetic Mn^{4+} ion in MnO_6 structure has a certain spin parity in the formed molecular orbitals^{10,26}. Here is our description for an appropriate realization of detected Mn^{4+} ion's spin quantum state, which is dealt with ferromagnetism empirically rationalized to intricate electronic hybridization in MnO_6 complex referring to PJTE²⁷. Formation of two-level system is taken into account in the two minima on *APES* in the mechanism of highest-occupied-molecular-orbital (*HOMO*) and lowest-unoccupied-molecular-orbital (*LUMO*) coupling.^{10,26–29}

B. ESR spectroscopy experiment using WG modes:

Field confinement of the WG mode in $SrLaAlO_4$ crystal allows loss mechanisms to be minimized to achieve a high Q-factor at 20 *mK*^{30–33}, which is required for an ultrasensitive ESR spectroscopy. Using X-band to Ku-band frequency WG multi-mode ESR at this temperature, high precision is achieved in the measurements of the spin-Hamiltonian parameters^{34,35}. Different process are devoted in measuring sensitivity of different type of resonator of wide range of frequency with varieties of probing system^{36–40}. Benmessai et al.⁶ described a concentration level measurement process of Fe^{3+} impurity ion exciting WG modes at millikelvin temperatures in sapphire. Anders et al.³⁹ described a single-chip electron spin resonance detector operating at 27 *GHz*.

For such a spectroscopy, a cylindrical light yellow $SrLaAlO_4$ single crystal of height 9.04 *mm* and diameter 17.18 *mm* was inserted centrally in an oxygen-free cylindrical copper cavity. The crystal loaded cavity was cooled in a dilution refrigerator (DR) to less than 20 *mK*. Practically microwave-power and other terms are kept constant then the required minimum number of impurity ion follows the proportionality²³ $N_{min} \propto \frac{1}{\omega Q_L}$ for detection of ESR transition spectrum. The required minimum spin number is estimated generally as:

$$N_{min} = \left(\frac{3K_B V_s T_s}{g_e^2 \beta^2 \mu_o S(S+1)} \right) \left(\frac{\Delta\omega}{\omega} \right) \left(\frac{1}{\eta Q_L} \right) \left(\frac{P_n}{P} \right)^{\frac{1}{2}} \quad (1)$$

Where V_s is the mode volume, T_s is the sample temperature, S is the electron effective spin, g_e is the electron g-factor, β is the Bohr electron magneton, μ_o is the magnetic permeability of free space, ω is the resonance frequency, η is the filling factor, P_n is the noise power at the detector, P is the microwave input power, and $\Delta\omega$ is the width of aggregated spin frequency at resonance which is depended on the shape-function $f(\omega)$ normalized as $\int_0^\infty f(\omega) d\omega = 1$ for a wide range of Larmor precession (ω_L) of magnetic dipoles²². Significant output (transmission) occurs only at resonance in a very narrow frequency width $\Delta\omega$ in the region $\omega \approx \omega_L$ at ESR. In this experiment, for Mn^{4+} ion $\Delta\omega \simeq 40$ *kHz* (red band in the Fig. 1). The variation of Q-factor was small due to a little dielectric variation among the selected modes, and observed loaded Q-factor Q_L was always more than

50,000 at 20 *mK*. Assuming, $\Delta\omega$ in the order of the line-width of all the selected WG modes, the minimum number of detectible ions setting $\frac{P_n}{P} \approx 1$ (see Eq.1) may be as low as 0.1 *ppb* level of concentration.

Fifteen WG modes with high-azimuthal-mode-number with a frequency range of 7 *GHz* to 18 *GHz*, and thus electromagnetic energy filling factors of order unity were monitored. The static magnetic field between -0.2 *T* to 1 *T* was varied through the use of computer control in a step of sweep 4×10^{-4} *T*. Each WG mode was scanned for a period of five seconds at each step of magnetic field sweep. This slow sweep of magnetic field was applied under control of an in-house MATLAB program to avoid heating above 20 *mK*, with the microwave input power of -60 *dBm*.

To avoid the addition of thermal noise from room temperature, a 10 *dB* microwave attenuator was used at 4 *K* stage and another one at 1 *K* stage of the DR. Also, a 20 *dB* attenuator was added at 20 *mK* stage of the DR. These cold stage attenuation plus the use of a low noise temperature cryogenic amplifier after the resonator ensures good enough signal to noise ratio (*SNR*). From this multi-mode ESR characteristics with hyperfine structure plotting as a map (Fig.2), we were able to identify the types of paramagnetic impurities present in the crystal.

C. Results and Discussion

Using the prescribed technique of experiment, the monitored ESR spectrum is mapped as in Fig-2. The isoelectronic Cr^{3+} ion of Mn^{4+} ion⁴¹ has a nuclear spin $I = \frac{7}{2}$, but manganese has nuclear spin $I = \frac{5}{2}$ which is responsible for hyperfine structure of 6-lines (Fig. 1, 2 and 3). The observed ESR spectrum assures the presence of Mn^{4+} ion in the $SrLaAlO_4$ crystal lattice. Optical spectroscopy study of Zhyachevskii et al.¹² shows that manganese ion is present exclusively in doped $SrLaAlO_4$ crystal tetragonal lattice in the form of Mn^{4+} ion occupying six fold coordinated Al^{3+} sites. Hence the presence of Mn^{4+} ion in lower valence Al^{3+} site is enhanced¹³. Also, the higher valence state of Mn^{4+} ion resulting in stronger Coulomb interaction between Mn^{4+} ion and O^{2-} ion^{12,13}. The fact that in the $^4T_{2g}$ triplet, Mn^{4+} ion has energy level overlapping depending on local charge density^{12,13}. This overlapping in the perovskite crystal SLA structure display variety of magnetic properties as a linear combinations of the atomic Hartree-Fock orbitals^{14,15,42,43} in the molecular orbitals (MO) of MnO_6 complex^{15,16}.

Some anisotropy of *g*-factors and hyperfine line space broadening is observed, opposite to the direction of the increase of applied DC magnetic field (Fig. 2 and 3). The geometrical anisotropy terms of the single MnO_6 structure is an important case where local order, as established by local interactions, cannot be freely propagated throughout space. The system can lift degeneracy resulting charge or spin ordering of manganese ion^{44,45}.

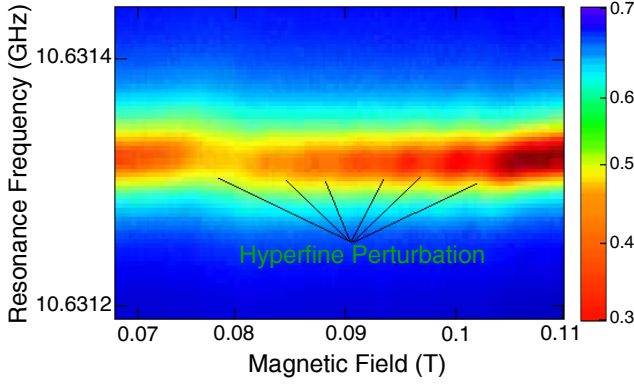


FIG. 1. Transmission spectrum colour density plot of Mn^{4+} ion nuclear spin perturbation with $WGH_{5,1,1}$ mode of resonance frequency 10.6313 GHz.

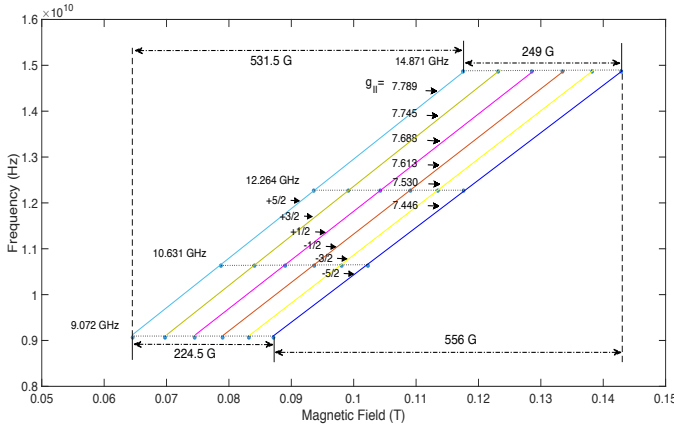


FIG. 2. g -factor map of Mn^{4+} ion ESR spectroscopy showing hyperfine structure broadening. Six lines of nuclear magnetic quantum numbers $+\frac{5}{2}, +\frac{3}{2}, +\frac{1}{2}, -\frac{1}{2}, -\frac{3}{2}$ and $-\frac{5}{2}$ shows different g -factors.

Crystal distortion relates to Jahn-Teller distortion⁴⁶, and metal-ligand charge transfer with orbital ordering plays an essential role in stabilizing ferromagnetic states^{10,28,45}.

The measured parallel g -factors decreases in the order of nuclear magnetic quantum number $+\frac{5}{2}, +\frac{3}{2}, +\frac{1}{2}, -\frac{1}{2}, -\frac{3}{2}, -\frac{5}{2}$ with the increase of magnetic field (Fig. 2 and 3). Measured parallel g -factors are $g_{||Mn} = 7.789, 7.745, 7.688, 7.613, 7.530$ and 7.446 according to the order $+\frac{5}{2}$ to $-\frac{5}{2}$. Similarly, hyperfine line spacings are $A_{||Mn} = -209.8 \times 10^{-4} \text{ cm}^{-1}, -196.4 \times 10^{-4} \text{ cm}^{-1}, -182.7 \times 10^{-4} \text{ cm}^{-1}, -169.1 \times 10^{-4} \text{ cm}^{-1}, -159.7 \times 10^{-4} \text{ cm}^{-1}, -153.7 \times 10^{-4} \text{ cm}^{-1}$ according to the order of nuclear magnetic quantum number $+\frac{5}{2}$ to $-\frac{5}{2}$ at 10.6313 GHz ($WGH_{5,1,1}$) (Fig. 2 and 3).

The crystal field created large gap between t_{2g} and e_{2g} stabilizing 4+ oxidation stage of manganese ion⁴⁷. It is a worthy remark that, in principle, any decrease in MnO_6 symmetry results in at least partial lifting of the orbital degeneracy, no matter how small the displacements are. Also, it has been observed by ESR in

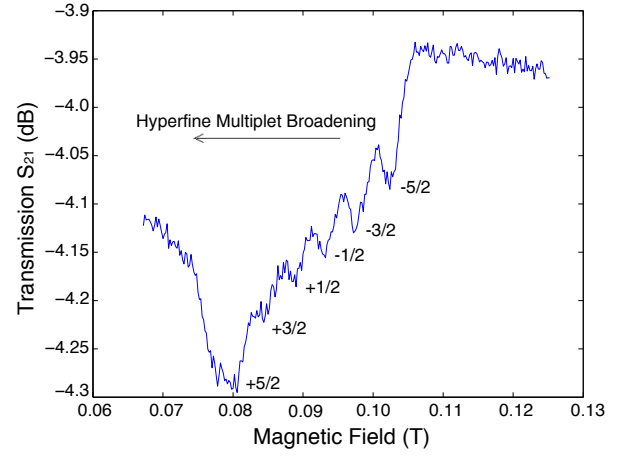


FIG. 3. ESR spectrum of $WGH_{5,1,1}$ mode of resonance frequency 10.6313 GHz. Spectrum of hyperfine line shows average spacing 44.16 G ($-178.5 \times 10^{-4} \text{ cm}^{-1}$) of Mn^{4+} ion at 20 mK.

$PbTiO_3$ that valence state of doped manganese in Ti^{3+} site changes from Mn^{2+} to Mn^{4+} with increase of its concentration²¹. This is usually accompanied by a distortion of crystal structure, typically through an interaction with the lattice⁴⁸. Likewise any orbital degeneracy lifting in the crystallographic sites due to structural distortion is bound to entail differences in the total electron charges leading to a non-integer oxidation state. Plausibly, elongated MnO_6 octahedron due to tetragonal distortion in $SrLaAlO_4$ may implies on the modulation of charge density and variation of oxidation in the covalency state of the Mn^{4+} ion extra charges in the substituted Al^{3+} ion sites^{20,47}. The tetragonal elongation (along c -axis) is 0.236 Å in the Al^{3+} site oxygen octahedron of two bonds $Al-O_2$ of length $R_{||} = 2.121$ Å and four coplanar bonds $Al-O_1$ of length $R_{\perp} = 1.885$ Å between aluminium and oxygen^{49,50}. As an instance, it may be mentioned that about 100 cm^{-1} energy change in average can be caused by 0.01 Å off-center displacement of the impurity ion (due to structural distortion)⁵¹. This crystal may have a little rhombic distortion at 20 mK temperature and is not identified as a ferroelectric crystal.

Observed giant g -factor indicates high magnetic moment of electron in the Mn^{4+} site at 20 mK. ESR spectrum reveals this magnetization state directly as a spin-Hamiltonian parameter rationalizing to intricate electronic hybridization. In this hybridization, paramagnetic ion's three phenomena ferro-electricity, magnetization, and spin-crossover are observed as coexisted¹⁰. Empirically, giant g -factor due to ferromagnetic two-level system which is formed in two potential minima on the APES between metal Mn and ligand O due to HOMO and LUMO coupling (Fig.4). The octahedral central manganese ion shifting with respect to oxygen $\mathbf{Q}_\alpha = (Q_x, Q_y, Q_z)$ in normal coordinates creates MnO_6 structural insta-

bility under a condition that the curvature of resultant spring constant $K = (\frac{\partial^2 E}{\partial Q_\alpha^2})_o$ (deviating from cubic symmetry) negative^{10,52}. $E = \langle \psi_o | H | \psi_o \rangle$ the energy at high-symmetry (cubic), the ground state wave function is ψ_o and H is the metal-ligand interaction Hamiltonian.

We consider that $K = K_o + K_v$. Where¹⁰;

$$K_o = \left\langle \psi_o \left| \left(\frac{\partial^2 H}{\partial Q_\alpha^2} \right)_o \right| \psi_o \right\rangle \quad (2)$$

is the ground state diagonal matrix element. It describes the fixed (rigid) nucleus high symmetry electron density distribution $|\psi_o|^2$ reflecting stiffness of the lattice as a long-range (whole crystal) feature. Whereas, the term K_v is always negative due to the Born-Oppenheimer ground state wave function and does not include long-range inter-cell interaction. This off-diagonal matrix elements are described in terms of second order perturbation as:^{27,52}

$$K_v = -2 \sum_n \frac{|\langle \psi_o | (\frac{\partial H}{\partial Q_\alpha})_o | \psi_n \rangle|^2}{E_n - E_o} \quad (3)$$

Instability arises in the structure under the condition $K_o + K_v < 0$ in strong enough PJTE lower-symmetry due to manganese ions additional covalency with oxygen. We can consider that K_o and K_v cancel one another approximately⁵². This allows us to focus on electronic interaction Hamiltonian for valence electrons only. In case of MnO_6 elongated (along z-axis) octahedron forming molecular orbitals as a linear combination of single electron Hartree-Fock wave function, the structure has attained the PJTE state of vibronic coupling at 20 mK. The HOMO is t_{1u} energy level of oxygen p_π function and LUMO is t_{2g} energy level of Mn^{4+} ion d_π function in hybridization⁵². Referring the wave functions ψ_o and ψ_n to HOMO and LUMO respectively, the vibronic coupling constant of PJTE for Mn^{4+} ion additional covalency can be given as:^{52,10,27}

$$F = \left\langle 2p_z(O) \left| \left(\frac{\partial H}{\partial Q_x} \right)_o \right| 3d_{yz}(Mn) \right\rangle \quad (4)$$

This perturbation forms a two-level system in the profile of APES (Fig.4).

The local character of the negative K_v contribution to the curvature indicates that the instability producing PJTE is essentially of local origin, and the long range (whole crystal) interaction of K_o is important in realization of instability condition $|K_v| > K_o$. This means that the PJTE of manganese ion center can be taken into account as two-level system²⁷ approximately reducing the denominator of the equation-3. Evidence of this instability reveals by the increased energy (or frequency) of spin transition in ESR due to higher magnetization of the ion Mn^{4+} creating giant g-factor as observed in the experiment. In such a two-level state, higher frequency WG mode ESR transmissions should be noisy, and observed same results as shown in the figure-5a,b,c,d. The

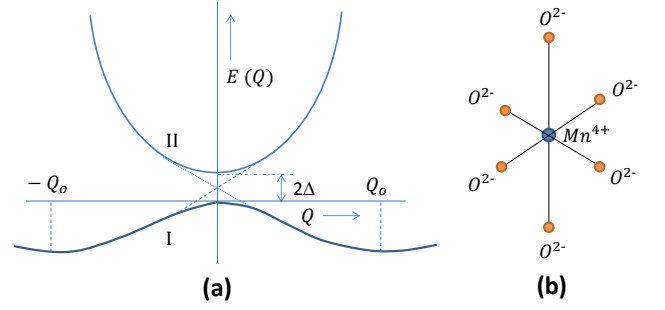


FIG. 4. - (a) Two-level system with two minima on APES at $+Q_o$ and $-Q_o$ due to PJTE at $\frac{F^2}{K_o} > \Delta$ state (Δ is the energy gap) of distortion in normal mode $Q = Q_\alpha(Q_x, Q_y, Q_z)$. At JTE stage the profiles are joining along dotted crossing lines: one from left to up right another from right to up left in a single distortion mode. (b) Elongated MnO_6 octahedral four-fold axes shape.

d^3 electron configuration of Mn^{4+} ion effective spin state $S = \frac{3}{2}$ in the t_{2g} orbital triplet is realised in the high crystal field of $SrLaAlO_4$. In contrast, according to the observed ESR spectrum of giant g-factor and low fine structure term, neither high-spin (HS) state $S = \frac{5}{2}$ nor low-spin (LS) state $S = \frac{1}{2}$ of d^5 electron of Mn^{2+} ion is to be considerable in this substantially elongated MnO_6 octahedral structure at 20 mK temperature. Therefore, considering the typical molecular-orbital in energy scheme of d^3 electron spin configuration, the HOMO is $(t_{1u} \downarrow)^3(t_{1u} \uparrow)^3(t_{2g} \uparrow)^3$ with the ground state term $^4A_{1g}$ and the LUMO is $(t_{1u} \downarrow)^2(t_{1u} \uparrow)^3(t_{2g} \uparrow)^3(t_{2g} \downarrow)^1$ with the lowest ungerade term $^4T_{1u}$ of odd parity^{10,52}. This ground and excited states of opposite parity mediates the two-level vibronic coupling in the PJTE. An important feature is that it takes place as a magnetic dipolar effect in the MnO_6 complex.

The measured high parallel g-factor $g_{\parallel Mn}$ of Mn^{4+} ion ESR in $SrLaAlO_4$ may compare with Suchocki et al.⁵³ observed enhanced zeeman effect with an effective g-factor in the range about 6 to 8 for Mn^{4+} ion in gadolinium gallium garnet (GGG) at 25 mK. It includes the degree of localization of the extra electron of Mn^{4+} ion, and indicates that spin transition has magnetic impedance due to inherent 'frustration' coupling.

The excess positive charge of Mn^{4+} increases its Coulomb force on the O^{2-} surrounded site, and cause of orbital energy reduction. Meddey et al.⁵⁴ claimed evidence of oxygen-vacancy induced ferromagnetic order of Mn^{4+} ion in the Mn doped $SrTiO_3$ single crystal. Oxygen vacancy or deficiency ($\delta = 0.15$) in the sample is formed as $SrTi_{1-x}Mn_xO_{3-\delta}$, and its ferromagnetic phase shows a clear hysteresis loop at low temperature^{54,55}. Hence, the excess positive charge of Mn^{4+} in the MnO_6 elongated octahedral sites of $SrLaAlO_4$ substituting Al^{3+} having oxygen deficiency creates order-disorder state in ferromagnetic phase and interacts with external applied magnetic field of ESR

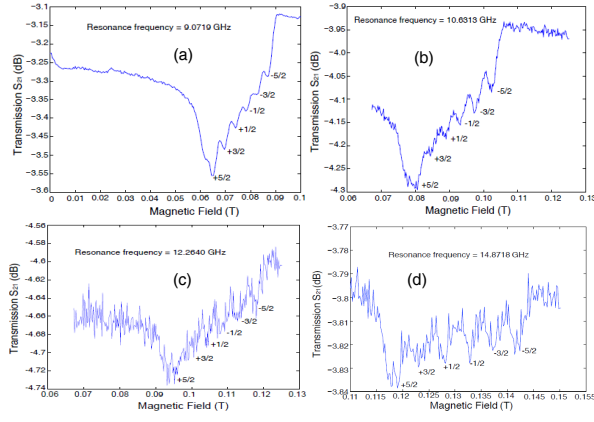


FIG. 5. Noisy hyperfine perturbation of Mn^{4+} ion ESR spectrum due to magnetic impedance of mode frequency with the increase of frequency 9.0719 GHz to 14.8718 GHz arises in cascade due to coupling with ferromagnetic two-level system of higher local magnetization respectively. Also, slope of the electron transmission among consecutive nuclear spin perturbation is lowering with the increase of frequency. Figure-(a) shows clear hyperfine structure and ESR transmission spectrum, and stiff slope of electron transmission spectrum among consecutive nuclear spin hyperfine coupling.

spectroscopy. Typically, another example of oxygen vacancy mechanism for the reason of observed giant g -factor is as Gorni et al⁵⁶ reported in their X-band parallel mode ESR experiment that the g -factor of manganese is 8.1 including 6.6 mT hyperfine structure line spacing at 5 K, centered at 86 mT. More clearly, the resonant frequency with applied external DC magnetic field \mathbf{B} parallel to the crystal axis may be given by the Kittel formula⁵⁷ $\omega = \gamma\sqrt{B(B + \mu_0 M)}$. Where M is the magnetization of the ferromagnet and γ is the gyromagnetic ratio. As a result, determination of g -factor depends on the relative spin and orbital moments of a material which can be evaluated by use of the well-known relation⁵⁷ $\frac{\mu_F}{\mu_S} = \frac{g-2}{2}$. Where, μ_F is the moment of spin in ferromagnetic state, and $\mu_S = \mu_B$ is the free spin moment.

Hence, we observed a giant g -factor as ESR is observed at higher resonance frequency with applied DC magnetic field B in addition with local magnetization M . In such a local environment with intricate electronic hybridization, measured nuclear hyperfine parameter is $P_{\parallel} \simeq -3.7 \times 10^{-4} \text{ cm}^{-1}$ as an impact of nuclear second order perturbation (calculated using spin Hamiltonian). Using the value of manganese nuclear quadrupole moment⁵⁸ $Q = +0.33(1) \text{ barn}$, the measured mean inverse third power of the electron distance is $\langle r_q^{-3} \rangle = 3.325 \text{ a.u.}$ at 20 mK. According to the theory, this term is approximately 10 – 20% higher in values for unfilled d -shell unpaired electrons. Ionic radius of Mn^{4+} ion in octahedral structure $r_{oh} = 0.67 \text{ \AA}$ is in good agreement with these measurements⁵⁹.

Although, Prodi et al presented that with temperature, mixed-valence manganites with the ABO_3 per-

ovskite structure display variation of properties with the relative concentration of Mn^{3+} and Mn^{4+} in the octahedral corner-sharing network⁴². Instead of this mixed-valence sites, we may consider this case in the insulated single MnO_6 structure taking into account a non-integer oxidation state of Mn^{4+} ion reducing from the 4+ oxidation state. The spin still reasonably same as it was in case of d^3 electron configuration in orbital triplet with high energy gap between e_g and t_{2g} . Although, spin-crossover mediates in orbital ordering resulting to structural change^{60,61}. Without of spin-crossover, the orbital triplet splitting is viable for d^3 configuration taking into account only the excited (lifted) $|xz\rangle$ and $|yz\rangle$ states of t_{2g} orbital triplet in the elongation along z -axis.

It is observed that the hyperfine perturbation becomes noisy with the increase of resonance frequency (Fig.5a,b,c,d). Apparently, the magnetic impedance due to ferromagnetic order induces the electron spin transitions. Increase of magnetic reminiscence in the ferromagnetic hysteresis loop can deplete the distinction of spin interactions. Both the ferroelectric order and ferromagnetic order has hysteresis loop in the above mentioned metastable two-level system of order-disorder phase. Although, the experimental results reveals the impact of magnetic impedance but not able to identify the accurate scale of ferromagnetic two-level system of order-disorder.

Regarding this two-level system, one electron Hamiltonian can be presented as $H = H_o + H_P$ with the part of PJTE perturbation H_P . In the second quantization formation due to Mn^{4+} ion and O^{2-} ion (HOMO and LUMO) electronic coupling, it is described with raising operator $a_i^\dagger(O_\mu)$ and lowering operator $a_j(O_\nu)$ as⁵²-

$$H_P = \sum_{\alpha} \sum_{\mu, \nu} \sum_{i, j} \left\langle i, O_{\mu} \left| \frac{\partial H}{\partial Q_{\alpha}} \right| j, O_{\nu} \right\rangle Q_{\alpha} a_i^\dagger(O_{\mu}) a_j(O_{\nu}) \quad (5)$$

Where; μ, ν denotes different atoms and i, j denotes different orbitals of coupling. Also, O_{μ} and O_{ν} denotes octahedral symmetry of the orbitals.

D. Conclusion:

The elongated MnO_6 octahedral structure become unstable in lower symmetry raising metastable two-level system on the APES at 20 mK. WG multi-mode ESR probes this instability directly revealing the Mn^{4+} ion's valence electron states in situ. Structural anisotropy and oxygen deficiency has the vital role in formation of metastable two-level system in electronic hybridisation state which has been explained in terms of vibronic theory of HOMO and LUMO coupling. Hyper fine line width broadening measurement and covalent effect is important for microscopic state analysis at millikelvin temperatures revealing nuclear dipolar hyperfine parameter (P_{\parallel}) and mean inverse third power of the electron distance $\langle r_q^{-3} \rangle$. Measured value of P_{\parallel} is negative as manganese

nuclear electric quadrupole moment is positive. Whereas, the value of P_{\parallel} is positive for Cu^{2+} ion in the same site as copper nuclear electric quadrupole moment is negative⁸.

Typically, in the formation of two-level system, bonding and anti-bonding mechanisms^{15,16} are involved in the linear combination of MO in the MnO_6 complex^{26,62}. WG mode ultrasensitive ESR spectroscopy probes these variety of intricate electronic local nature of magneto-electric effects with high precision.

ACKNOWLEDGMENTS

This work was funded by Australian Research Council (ARC), Grant no. CE110001013. Thanks to Dr. Warrick Farr for assistance with data acquisition and Mr. Steve Osborne for making cavity.

E. References:

- ¹G. Kurizki^{a,1}, P. Bertet^b, Y. Kubo^b, K. Mlmer^c, D. Petrosyan^{d,e}, P. Rabl^f, and J. Schmiedmayer^f, PNAS **112**, 3866 (2015).
- ²R. Dumke^{1,2,12}, Z. Lu³, J. Close⁴, N. Robins⁴, A. Weis⁵, M. Mukherjee^{2,6}, G. Birkel⁷, C. Hufnagel², L. Amico^{2,8,9}, M. G. Boshier¹⁰, K. Dieckmann², W. Li^{2,6}, and T. C. Killian¹¹, J. Opt. **18** (2016).
- ³G. Binsky, R. Amsuss, J. Majer, D. Petrosyan, J. Schmiedmayer, and G. Kurizki, Quantum Inf Process **10**, 1037 (2011).
- ⁴N. Klinduhov and K. Boukheddaden, J. Phys. Chem. Lett. **7**, 722 (2016).
- ⁵W. G. Farr, D. L. Creedon, M. Goryachev, K. Benmessai, and M. E. Tobar, Phys. Rev. B **88**, 224426 (2013).
- ⁶K. Benmessai, W. G. Farr, D. L. Creedon, Y. Reshitnyk, J.-M. Le Floch, T. Duty, and M. E. Tobar, Phys. Rev. B **87**, 094412 (2013).
- ⁷I. Buluta, S. Ashhab, and F. Nori, Rep. Prog. Phys. **74**, 104401 (2011).
- ⁸M. A. Hosain, J. -M. Le Floch, J. Krupka, and M. E. Tobar, J. Magn. Reson. **281**, 209 (2017).
- ⁹I. B. Bersuker, Chemical Review **113**, 1351 (2013).
- ¹⁰I. B. Bersuker, Physical Review letters **108**, 137202 (2012).
- ¹¹S. ichi Ohkoshi, K. Imoto, Y. Tsunobuchi, S. Takano, and H. Tokoro, Nature Chemistry **3**, 564 (2011).
- ¹²Y. Zhydashkevskii, A. Suchocki, A. Paja. czkowska, A. Kos, A. Szysiak, and A. Reszka, Optical Materials **35**, 1664 (May 2013).
- ¹³E. Talika, A. P. czkowskab, A. Guzika, P. Zajdela, J. Kusza, A. Kosb, and A. Szysiakb, Materials Science and Engineering B **182**, 74 (2014).
- ¹⁴T. Gupta and G. Rajaraman, Chem. Cmmun. **52**, 8972 (2016).
- ¹⁵A. Palii, B. Tsukerblat, J. M. Clemente-Juan, and S. M. Aldoshin, J. Phys. Chem. A **119**, 9844 (2015).
- ¹⁶K. D. Demedis, C. M. Harshorn, and T. J. Meyer, Chem. Rev. **101**, 2655 (2001).
- ¹⁷R. Eichel, Phys. Chem. Chem. Phys. **13**, 368 (2011).
- ¹⁸S. R. Dunsiger, J. S. Gardner, J. A. Chakhalian, A. L. Cornelius, M. Jaime, R. F. Keifl, R. Movshovich, W. A. MacFarlane, R. I. Miller, J. E. Sonier, and B. D. Gaulin, Physical Review Letters **85**, 3504 (2000).
- ¹⁹P. G. Radaelli, New Journal of Physics **7**, 53 (2005).
- ²⁰R. Gupta, T. Taguchi, B. Lassalle-Kaiser, E. L. Bominaar, J. Yano, M. P. Hendrich, and A. S. Borovik, PNAS **112**, 5319 (2015).
- ²¹K. Hayashi, A. Ando, Y. Hamaji, and Y. Sakabe, Jpn. J. Appl. Phys **37**, 5237 (1998).
- ²²A. Abragam and B. Bleaney, *Electron Paramagnetic Resonance of Transition Ions* (Oxford University Press, 1970) Chap. Ions of the 3d group, pp. 365–490.
- ²³C. P. Poole Jr. and H. A. Franch, *Handbook of Electron Spin Resonance*, Vol. 2 (Springer-Verlag, New York, 1999) Chap. Sensitivity, pp. 3–12.
- ²⁴B. Bleaney, K. D. Bowers, and H. M. L. Pryce, Proc. R. Soc. Lond. **228**, 166 (1955).
- ²⁵C. Rudowicz, J. Phys.: Condens. Matter **12**, 417 (2000).
- ²⁶M.-H. Whangbo, E. E. Gordon, H. Xiang, H.-J. Koo, and C. Lee, Acc. Chem. Res. **48**, 3080 (2015).
- ²⁷I. B. Bersuker, Journal of Physics: Conference Series **428**, 012028 (2013).
- ²⁸L. Weston, X. Y. Cui, S. P. Ringer, and C. Stampfl, Physical Review B **93**, 165210 (2016).
- ²⁹A. Biancoli, C. M. Fancher, J. L. Jones, and D. Damjanovic, Nature Materials **14**, 224 (2015).
- ³⁰J. Krupka, K. Derzakowski, M. E. Tobar, J. Hartnett, and R. G. Geyer, Meas. Sci. Technol. **10**, 387 (1999).
- ³¹J.-M. Le Floch, J. D. Anstie, M. E. Tobar, J. G. Harnett, P.-Y. Bourgeois, and D. Cros, Physics Letters A **359**, 1 (2006).
- ³²M. Gomilsek, Seminar: University of Ljubljana, Slovenia, Year:2012. .
- ³³J. Krupka and J. Mazierska, IEEE Transactions On Microwave Theory And Techniques **48**, 1 (2000).
- ³⁴J. R. Pilbrow, *Transition Ion Electron Paramagnetic Resonance* (Oxford University Press, Walton Street, Oxford OX2, UK, 1990) Chap. 1, pp. 3–61.
- ³⁵B. Bleaney, K. Bowers, and D. Ingram, Proc. R. Soc. Lond. **228**, 147 (1955).
- ³⁶G. Annino, M. Cassettari, I. Longo, and M. Martinelli, Appl. Magn. Reson. **16**, 45 (1999).
- ³⁷I. Longo, Meas. Sci. Technol. **2**, 1169 (1991).
- ³⁸A. Colligiani, Appl. Magn. Reson. **15**, 39 (1998).
- ³⁹J. Anders, A. Angerhofer, and G. Boero, Journal of Magnetic Resonance **86217**, 19 (2012).
- ⁴⁰Y. S. Yap, Y. Tabuchi, M. Negoro, and A. Kagawa, Review of Scientific Instruments **86**, 0631101 (2015).
- ⁴¹B. Henderson and T. P. P. Hall, Proc. Phys. Soc. **90**, 511 (1967).
- ⁴²A. Porodi, E. Giloli, A. Gauzzi, F. Licci, M. Marezio, F. Bolzoni, Q. Huang, A. Santoro, and J. Lynn, Nature Materials **3**, 48 (2004).
- ⁴³Y. Shimakawa, S. Zhang, T. Saito, M. W. Lufaso, and P. M. Woodward, Inorg. Chem. **53**, 594 (2014).
- ⁴⁴Y. Murakami, H. Kawada, H. Kawata, M. Tanaka, T. Arima, Y. Morimoto, and Y. Tokura, Phys. Rev. Lett. **80**, 1932 (2 March 1998).
- ⁴⁵T. Mizokawa and A. Fujimori, Phys. Rev. B **56**, R493 (1997).
- ⁴⁶M. A. Hosain, J.-M. L. Floch, J. Krupka, and M. E. Tobar, J. Phys.: Condens. Matter **30**, 015802(8pp) (2017).
- ⁴⁷M. Du, ECS Journal of Solid State Science and Technology **5(1)**, R3007 (2016).
- ⁴⁸D. I. Khomskii and M. V. Mostovoy, J. Phys. A: Math. Gen. **36**, 9197 (2003).
- ⁴⁹P. Aleshkevych, M. Berkowski, W. Ryba-Romanowski, and H. Szymczak, Phys. Stat. sol. (b) **218**, 521 (2000).
- ⁵⁰W.-H. Wei, S.-Y. Wua, and H.-N. Dongb, Z. Naturforsch **60a**, 541 (March 2005).
- ⁵¹Y. V. Yablokov and T. A. Ivanova, Coordination Chemistry Reviews **190-192**, 1255 (1999).
- ⁵²V. Polinger, P. Garcia-Fernandez, and I. B. Bersuker, Physica B **457**, 296 (2015).
- ⁵³A. Suchocki, S. Biernacki, G. Boulon, A. Brenier, M. Potemski, and A. Wyszomolek, Chemical Physics **298**, 267 (2004).
- ⁵⁴S. Middey, C. Meneghini, and S. Ray, Applied Physics Letters **101**, 042406 (2012).
- ⁵⁵D. Choudhury, B. Pal, A. Sharma, S. V. Bhat, and D. D. Sarma, Scientific Report **3**, 1433 (2013).

- ⁵⁶S. Gorni, G. Blain, R. Guillot, C. Policar, and E. Mallart, *Inorganic Chemistry* **46**, 1951 (2007).
- ⁵⁷C. Kittel, *Phys. Rev.* **76**, 743 (1949).
- ⁵⁸N. Stone, *Atomic Data and Nuclear Data Tables* **90**, 75 (2005).
- ⁵⁹R. D. SHANNON, *Acta. Cryst.* **A 32**, 751 (1976).
- ⁶⁰N. C. Bristowe, J. Varignon, D. Fontaine, E. Bousquet, and P. Ghosez, *Nature Communications* **6**, 6677 (2015).
- ⁶¹J.-H. Park, E. Vescovo, H.-J. Kim, C. Kwon, R. Ramesh, and T. Venkatesan, *Nature* **392**, 794 (1998).
- ⁶²X.-X. Wu and W.-C. Zheng, *Appl. Magn. Reson.* **46**, 85 (2015).